



Helical dynamo growth and saturation at modest versus extreme magnetic Reynolds numbersHongzhe Zhou **Tsung-Dao Lee Institute, Shanghai Jiao Tong University, 800 Dongchuan Road, Shanghai 200240, People's Republic of China and Nordita, KTH Royal Institute of Technology and Stockholm University, Hannes Alfvéns väg 12, SE-10691 Stockholm, Sweden*Eric G. Blackman[†]*Department of Physics and Astronomy, University of Rochester, Rochester, New York 14627, USA and Laboratory for Laser Energetics, University of Rochester, Rochester, New York 14623, USA* (Received 12 February 2023; revised 18 July 2023; accepted 21 December 2023; published 19 January 2024)

Understanding magnetic field growth in astrophysical objects is a persistent challenge. In stars and galaxies, turbulent flows with net kinetic helicity are believed to be responsible for driving large-scale magnetic fields. However, numerical simulations have demonstrated that such helical dynamos in closed volumes saturate at lower magnetic field strengths when increasing the magnetic Reynolds number Rm . This would imply that helical large-scale dynamos cannot be efficient in astrophysical bodies without the help of helicity outflows such as stellar winds. But do these implications actually apply for very large Rm ? Here we tackle the long-standing question of how much helical large-scale dynamo growth occurs independent of Rm in a closed volume. We analyze data from numerical simulations with a new method that tracks resistive versus nonresistive drivers of helical field growth. We identify a presaturation regime when the large-scale field grows at a rate independent of Rm , but to an Rm -dependent magnitude. The latter Rm dependence is due to a dominant resistive contribution, but whose fractional contribution to the large-scale magnetic energy decreases with increasing Rm . We argue that the resistive contribution would become negligible at large Rm and an Rm -independent dynamical contribution would dominate if the current helicity spectrum in the inertial range is steeper than k^0 . As such helicity spectra are plausible, this renews optimism for the relevance of closed dynamos. Our work pinpoints how modest Rm simulations can cause misapprehension of the $Rm \rightarrow \infty$ behavior.

DOI: [10.1103/PhysRevE.109.015206](https://doi.org/10.1103/PhysRevE.109.015206)**I. INTRODUCTION**

Large-scale magnetic fields are observed in planets, stars, and galaxies and play dynamically important roles in various astrophysical processes and phenomena including stellar evolution, galaxy formation, accretion and jet formation, and the engines of short gamma-ray bursts and kilonovae [1–4]. Such large-scale magnetic fields typically require an *in situ* dynamo mechanism to sustain against macroscopic and microscopic diffusion. Helical motion of turbulent eddies is a common driver of large-scale helical magnetic fields [5–9], known as the α effect. For closed-volume systems, both theory and simulations reveal that the late-time saturation of large-scale dynamo (LSD) is constrained by resistive effects, and hence is achieved on resistively long time scales [10–14].

While these results represent progress in understanding the time evolution of dynamo saturation in simple idealized

computational boxes, the dynamical times of real physical systems such as stars, galaxies, and accretion engines are much shorter than the resistive time scale given their very large magnetic Reynolds numbers Rm . It has thus remained an important and long-debated question as to whether significant large-scale fields can be generated by helical dynamo action for real astrophysical rotators. [15–22].

Astrophysical dynamo models have included helicity fluxes, e.g., Refs. [23–28], and anisotropic forcing [29] to alleviate the resistive constraint. (See Ref. [30] for a comprehensive review, and Refs. [31–34].) But a different solution without boundary fluxes would be an Rm -independent regime during the dynamical time scale of the dynamo before the resistive effects become dominant [11,35,36]. Whether this regime exists for high- Rm closed systems has been controversial, because in the numerical simulations of helical dynamos at accessible values of Rm , field strengths decrease with increasing Rm before the resistive phase. This would seem to challenge the dynamical quenching (DQ) formalism [11,23,37–40], where a significant large-scale field is expected before the resistive regime. In short, the modest values of Rm accessible in simulations have left previous analyses unable to separate dynamical and resistive dynamo phases, leaving ambiguity as to whether the measured field strengths and growth rates are dominated by the dynamical or resistive effects.

*hongzhe.zhou@sjtu.edu.cn

†blackman@pas.rochester.edu

Published by the American Physical Society under the terms of the [Creative Commons Attribution 4.0 International](https://creativecommons.org/licenses/by/4.0/) license. Further distribution of this work must maintain attribution to the author(s) and the published article's title, journal citation, and DOI. Funded by [Bibsam](https://www.bibsam.com/).

In this work, we tackle the problem in a new way. In particular, we track phases of the helical dynamo using normalized small-scale current helicity, rather than the bare time. We demonstrate that such a formulation facilitates identifying terms in the large-scale dynamo growth rate that are Rm independent and measurable in simulations, and reveals a prequenched (PQ) regime during which the growth rate is Rm independent at asymptotically large Rm. Interestingly, whether an Rm-independent saturation magnitude of large-scale fields at the end of the PQ regime exists for closed-volume helical dynamos depends crucially on the spectral slope of the underlying turbulent current helicity. In addition to the implications for astrophysical dynamos, this work also highlights the necessity of care required to avoid pitfalls when comparing the physical implications of large-scale dynamo and magnetohydrodynamical turbulence theories with simulations of limited magnetic Reynolds numbers.

The rest of this work is organized as follows. In Sec. II we introduce the numerical setup of helical dynamo simulations. In Sec. III we interpret simulation data with new analysis tools and in Sec. IV we seek for implications of its Rm dependence. Discussions and conclusions are in Sec. V.

II. NUMERICAL SETUP AND NONDIMENSIONALIZATION

We perform compressible magnetohydrodynamics simulations with an isothermal equation of state using the PENCIL CODE [41].

The equations to be solved are

$$\partial_t \rho + \nabla \cdot (\rho \mathbf{U}) = 0, \quad (1)$$

$$\begin{aligned} \partial_t \mathbf{U} + \mathbf{U} \cdot \nabla \mathbf{U} &= \frac{1}{\rho} [\mathbf{J} \times \mathbf{B} + \nabla \cdot (2\rho \nu \mathbf{S})] \\ &\quad - c_s^2 \nabla \ln \rho + \mathbf{f}, \end{aligned} \quad (2)$$

$$\partial_t \mathbf{A} = \mathbf{U} \times \mathbf{B} + \eta \nabla^2 \mathbf{A}, \quad (3)$$

where ρ , \mathbf{U} and \mathbf{A} are the density, the velocity, and the vector potential fields, respectively; $\mathbf{B} = \nabla \times \mathbf{A}$ is the magnetic field, $\mathbf{J} = \nabla \times \mathbf{B} / \mu_0$ is the current density with μ_0 being the vacuum permeability, and the units are chosen such that $\mu_0 = 1$; c_s is the constant and uniform sound speed; $S_{ij} = (\partial_i U_j + \partial_j U_i) / 2 - \delta_{ij} \nabla \cdot \mathbf{U} / 3$ is the rate-of-strain tensor; ν and η are the viscosity and resistivity, respectively; and finally \mathbf{f} is a fully helical forcing of the form of plane waves, with a fixed wave number k_f and random phase and direction at each time step. The simulation domain is a Cartesian box, with length of 2π and periodic boundary conditions in all three directions, and consequently the magnetic helicity becomes gauge invariant. For all runs, we use $k_f = 4$ and Mach numbers $\text{Ma} = u_{\text{rms}} / c_s \simeq 0.1$, where u_{rms} is the root-mean-square (rms) velocity. The Reynolds numbers $\text{Re} = u_{\text{rms}} / \nu k_f$ are kept roughly constant $\simeq 5$, and the magnetic Prandtl number $\text{Pm} = \nu / \eta$ is varied from 1 for run A1 to 80 for run A6. This isolates the Rm dependence from that of Re.

Without any mean flow, a helical dynamo generates fully helical large-scale fields. It is therefore most convenient to delineate the dynamo process using the magnetic helicity spectrum \mathcal{H}^M , which is gauge invariant given our periodic

boundary condition. We normalize energy and helicity spectra such that integration over all wave numbers yields the average energy or helicity density. We then decompose the large-scale magnetic helicity density into a mean handedness s_1 , a mean wave number k_1 , and the associated energy

$$\int_{k_0}^{k_f} \mathcal{H}_1^M dk = s_1 k_1^{-1} \int_{k_0}^{k_f} k |\mathcal{H}_1^M| dk, \quad (4)$$

where the subscripts 1 refer to large-scale modes, k_0 is the lowest wave number in the simulations,

$$s_1 = \frac{\int_{k_0}^{k_f} \mathcal{H}_1^M dk}{\int_{k_0}^{k_f} |\mathcal{H}_1^M| dk} \quad (5)$$

is the mean handedness and

$$k_1 = \frac{\int_{k_0}^{k_f} k |\mathcal{H}_1^M| dk}{\int_{k_0}^{k_f} |\mathcal{H}_1^M| dk} \quad (6)$$

is the mean wave number of the large-scale modes. Similarly, we decompose the small-scale (denoted by subscripts 2) magnetic helicity density as

$$\int_{k_f}^{\infty} \mathcal{H}_2^M dk = s_2 k_2^{-1} \int_{k_f}^{\infty} k |\mathcal{H}_2^M| dk, \quad (7)$$

$$s_2 = \frac{\int_{k_f}^{\infty} \mathcal{H}_2^M dk}{\int_{k_f}^{\infty} |\mathcal{H}_2^M| dk}, \quad (8)$$

$$k_2 = \frac{\int_{k_f}^{\infty} k |\mathcal{H}_2^M| dk}{\int_{k_f}^{\infty} |\mathcal{H}_2^M| dk}. \quad (9)$$

Note that $s_i \in [-1, 1]$ and $k_i > 0$ for $i = 1, 2$. The nondimensional energy density of the large-scale helical field is

$$\tilde{E}_L = \frac{1}{\rho u_{\text{rms}}^2} \int_{k_0}^{k_f} k |\mathcal{H}_1^M| dk. \quad (10)$$

We define the dimensionless time as

$$\tilde{t}(t) = \int_0^t u_{\text{rms}}(t') k_f dt', \quad (11)$$

and the dimensionless exponential growth rate

$$\tilde{\gamma} = \frac{d \ln \tilde{E}_L}{d \tilde{t}}. \quad (12)$$

III. RESULTS AND ANALYSIS

The LSD can be understood with the mean-field formalism, described by the mean-field induction equation. By taking the curl of Eq. (3) and averaging we obtain

$$\partial_t \langle \mathbf{B} \rangle = \nabla \times (\langle \mathbf{U} \rangle \times \langle \mathbf{B} \rangle + \mathcal{E}) + \eta \nabla^2 \langle \mathbf{B} \rangle, \quad (13)$$

where $\langle \cdot \rangle$ is an average over a scale assumed to be much larger than the turbulent forcing scale. We then use lower case \mathbf{b} to indicate the contribution to \mathbf{B} with zero mean, and similar constructions for the magnetic vector potential \mathbf{A} and velocity \mathbf{U} . The turbulent electromotive force (EMF) is $\mathcal{E} = \langle \mathbf{u} \times \mathbf{b} \rangle$. For statistically isotropic and homogeneous turbulence, $\langle \mathbf{U} \rangle = \mathbf{0}$ and the turbulent EMF takes the form $\mathcal{E} = \alpha \langle \mathbf{B} \rangle - \beta \nabla \times \langle \mathbf{B} \rangle$, where the turbulent diffusivity is $\beta =$

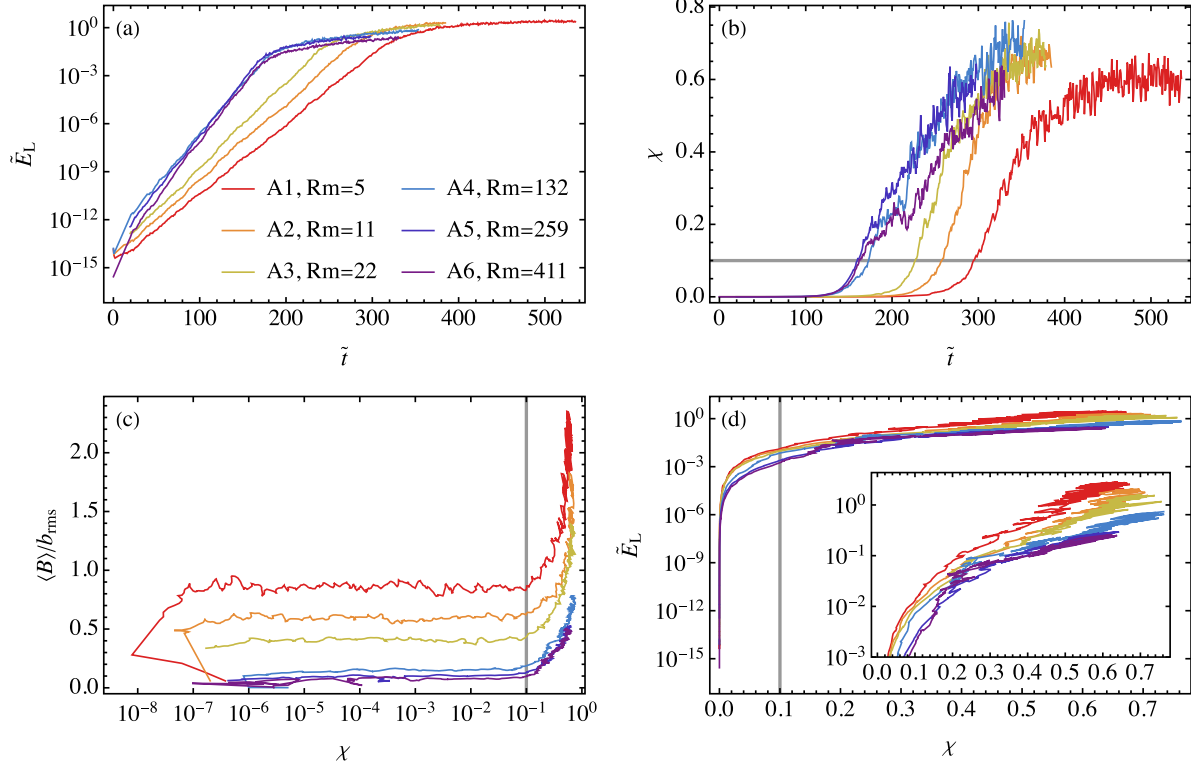


FIG. 1. Evolution of nondimensional quantities. (a) Normalized large-scale magnetic energy versus dimensionless time. (b) Dynamical quenching factor versus dimensionless time. (c) Ratio between the mean and fluctuating field strengths versus dynamical quenching factor. (d) Normalized large-scale magnetic energy versus dynamical quenching factor; the inset is a zoom-in plot. The horizontal line in panel (b) and the vertical lines in panels (c) and (d) denote the starting point of the LSD at $\chi = 0.1$.

$\tau u_{\text{rms}}^2/3$, and $\tau = 1/u_{\text{rms}}k_f$. The α coefficient is $\alpha = \alpha_k + \alpha_m$ given by the DQ formalism [11,37,38], where

$$\alpha_k = -\frac{1}{3} \left\langle \int_0^t \mathbf{u}(t) \cdot \nabla \times \mathbf{u}(t') dt' \right\rangle \simeq -\frac{1}{3} \epsilon u_{\text{rms}} \quad (14)$$

is the kinetic contribution, and

$$\begin{aligned} \alpha_m &= \frac{1}{3} \left\langle \int_0^t \mathbf{b}(t) \cdot \nabla \times \mathbf{b}(t') dt' \right\rangle \simeq \frac{1}{3} b_{\text{hel}} \\ &\simeq \frac{1}{3} \left(\int_{k_f}^{\infty} k \mathcal{H}_2^M dk \right)^{1/2} \end{aligned} \quad (15)$$

is the magnetic contribution. The latter is related to the small-scale current helicity density multiplied by a correlation time, and hence has the dimension of velocity in Alfvén units. b_{hel} is the helical part of the small-scale magnetic field and can be written in terms of the magnetic helicity spectrum \mathcal{H}^M as in Eq. (15). In Eq. (14), we have assumed the velocity field to be fully helical, which is consistent with our simulations. A factor ϵ is introduced to capture the possible deviation of the correlation time between \mathbf{u} and its curl, from the eddy turnover time $1/u_{\text{rms}}k_f$. Measuring ϵ can be method dependent and so we treat it as a free parameter. We shall see that $\epsilon = 0.8$ is sufficient to explain simulations, and more crucially, it has no influence on the implications on the Rm dependence of helical LSDs.

In the DQ formalism, α_m grows in time, offsets α_k , and eventually quenches the dynamo. We thus define

$$\chi \equiv -\epsilon \frac{\alpha_m}{\alpha_k} = u_{\text{rms}}^{-1} \left(\int_{k_f}^{\infty} k \mathcal{H}_2^M dk \right)^{1/2} \quad (16)$$

as the DQ factor, which is roughly the normalized current helicity, contains no free parameter, and is calculable from simulations. The measured values of χ fluctuate but grow nearly monotonically in time from ~ 0 to a value $\lesssim 1$ at the end of the LSD as expected from theory. In what follows, any quantity taken at $\chi = \chi'$ is meant to be its average over the interval $\chi \in [\chi' - \delta, \chi' + \delta]$ with $\delta = \min\{0.2\chi', 0.05\}$, unless otherwise specified.

In Fig. 1(a) we show the evolution of \tilde{E}_L tracked with the dimensionless time \tilde{t} measured in units of $1/u_{\text{rms}}k_f$ as in previous work. For sufficiently large Rm, a small-scale dynamo (SSD) is excited at early times and the growth of the large-scale modes is dominated by nonlinear intermode interactions rather than the interaction with the velocity field through the α effect. Figure 1(a) shows growth rates during the initial exponential stages (e.g., $0 \leq \tilde{t} \lesssim 300$ for run A1, $0 \leq \tilde{t} \lesssim 150$ for run A6, etc.) increases with increasing Rm, which is a signature SSD feature. Unambiguously pinpointing the end of the SSD phase is difficult on this plot but we next argue that using χ to track dynamo evolution alleviates this problem.

The SSD and LSD phases can be separated by considering their contributions to the small-scale current helicity. SSDs

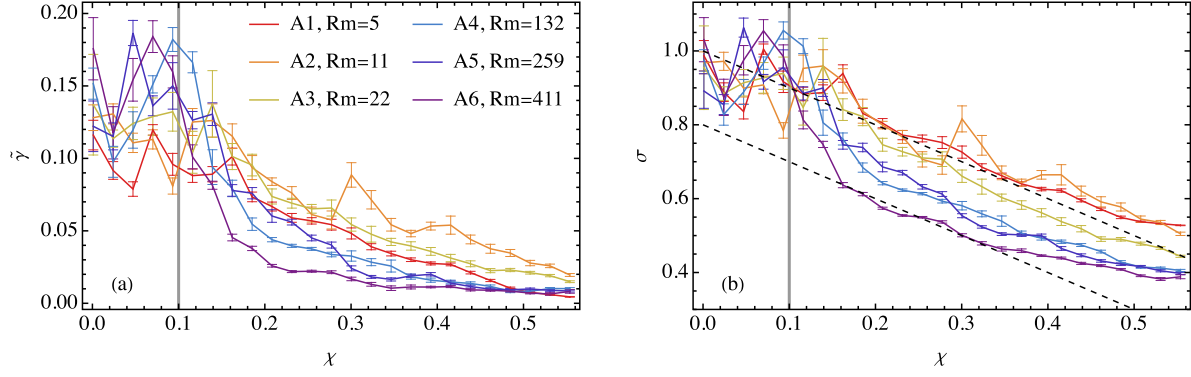


FIG. 2. (a) Normalized LSD growth rate $\tilde{\gamma}$ and (b) LSD efficiency σ versus the dynamical quenching factor χ . In both panels, the vertical dashed line at $\chi = 0.1$ indicates the start of the LSD phase. In panel (b), the two black dashed lines indicate the theoretical expectation $\sigma^{\text{th}} = \epsilon - \chi$ with different ratios of the time scales of α_k and β : $\epsilon = 1$ (upper) and $\epsilon = 0.8$ (lower).

efficiently amplify small-scale fields but with a low fractional magnetic helicity. This is supported by Fig. 1(b) which shows the evolution of χ (essentially the normalized small-scale current helicity) tracked by \tilde{t} . By comparing Figs. 1(a) and (b), we see that regardless of the Rm across different runs, the initial Rm-dependent exponential growth always corresponds to the $\chi \leq 0.1$ regime.

Figure 1(c) provides further support of using $\chi = 0.1$ to separate SSD and LSD phases, where we plot the ratio between the mean and the fluctuating field strengths tracked using χ . In the $\chi < 0.1$ region, this ratio remains roughly constant for all runs, suggesting that at this stage all the mean field growth is dominated by the low-wave number tail of a SSD growth, not a growing LSD. We therefore regard $\chi = 0.1$ as the onset of the LSD phases in what follows.

Finally, in Fig. 1(d) we show the evolution of \tilde{E}_L tracked by χ . Having identified the starting χ of the LSD, we must now identify its ending point after which resistive effects dominate, and quantify the Rm dependence of LSD growth and saturation. This requires detailed theoretical analysis, as explained in the following subsections.

A. LSD growth rate versus Rm

For a helical LSD without a mean flow (i.e., an α^2 dynamo), the energy growth rate of the mode at wave number k_1 is $\gamma = 2|\alpha|k_1 - 2(\beta + \eta)k_1^2$ [30]. Using Eqs. (14) and (15), the α coefficient can be written as $\alpha = \alpha_k + \alpha_m = -u_{\text{rms}}(\epsilon - \chi)/3$. Using the eddy turnover rate $u_{\text{rms}}k_f$ for normalization, we have the theoretical expectation

$$\tilde{\gamma}_{\text{th}} = \frac{\gamma}{u_{\text{rms}}k_f} = \frac{2k_1}{3k_f}(\epsilon - \chi) - \left(\frac{2}{3} + \frac{2}{\text{Rm}}\right)\left(\frac{k_1}{k_f}\right)^2, \quad (17)$$

where $\text{Rm} = u_{\text{rms}}/\eta k_f$ is the instantaneous magnetic Reynolds number. The LSD initially operates kinematically when $\chi \ll 1$, but is then dynamically quenched by χ due to the growing small-scale current helicity. The maximal value χ can obtain is analytically determined by $\tilde{\gamma} = 0$ to be $\epsilon - k_1/k_f$ when $\text{Rm} \rightarrow \infty$. This gives $\epsilon - k_0/k_f$ as the upper bound of χ at which LSD terminates.

The dimensionless growth rate $\tilde{\gamma}$ versus χ in simulations [defined in Eq. (12)] is plotted in Fig. 2(a). In principle, it should be compared with $\tilde{\gamma}_{\text{th}}$ in Eq. (17) to validate the DQ

formalism, based on which $\tilde{\gamma}_{\text{th}}$ is derived. However, the exact value of ϵ is yet unknown. Rather than fitting the data to find the most probable ϵ , we isolate the Rm-independent part in Eq. (17) by defining

$$\sigma = \frac{3k_f}{2k_1}\tilde{\gamma} + \left(1 + \frac{3}{\text{Rm}}\right)\frac{k_1}{k_f}. \quad (18)$$

Since the right-hand-side terms of Eq. (18) are all measurable, the values of σ from simulation data should collapse to set of Rm-independent straight lines determined by $\epsilon - \chi$ when $\text{Rm} \gg 1$ according to Eq. (17), assuming that ϵ is asymptotically Rm independent.

The right side of Eq. (18) is measured and plotted in Fig. 2(b) for different runs. Overall, the measured values of σ after the SSD phases at $\chi \geq 0.1$ can be well described by the theoretical expectation $(\epsilon - \chi)$, with $\epsilon \in [0.8, 1]$, as indicated by the two black dashed lines. This implies a modest 20% deficit in the correlation time between \mathbf{u} and its curl (which enters α_k) than that between \mathbf{u} and itself (which enters β), and might explain the submaximal LSD efficiency of Ref. [36]. Since the LSD phase should be bounded by $\epsilon - k_0/k_f$, we determine that

$$0.1 \leq \chi \leq 0.55 \quad (19)$$

quantitatively demarks the PQ regime whose Rm dependence we will assess.

The agreement between measured values and theoretical expectation of σ validates Eq. (17), and thus justifies that (i) the DQ formalism correctly describes the α^2 dynamo, and (ii) the LSD growth rate is asymptotically independent of Rm when $\text{Rm} \gg 1$. To see the latter point, notice that on the right of Eq. (17) the only two Rm-dependent quantities are Rm itself and k_1 . The k_1 is initially the value $\sim k_f/2$ which maximizes $\tilde{\gamma}$. Later, k_1 decreases to the lowest wave number available in the system, and this evolution may depend on Rm. But overall, k_1 always changes by a factor of $k_f L/4\pi$ if L is the length scale of the system, which is Rm independent. Hence the Rm dependence of $\tilde{\gamma}$ introduced by k_1 is quite weak and $\tilde{\gamma}$ will not decrease to some resistively small value.

Finally, we note that resistive diffusion of magnetic helicity reduces the growth rate of χ and thus slows the magnetic back reaction on the LSD, but does not directly show up in the LSD growth rate, Eq. (17). Hence at any given χ during the

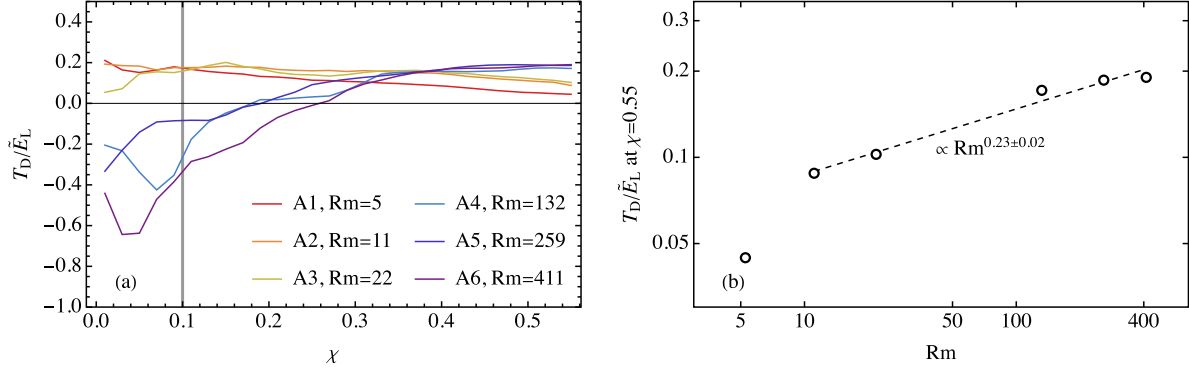


FIG. 3. Rm-dependent field strength in helical LSDs. (a) Fractional contributions to \tilde{E}_L from the dynamical term T_D/\tilde{E}_L from different runs. Hence $T_R/\tilde{E}_L = 1 - T_D/\tilde{E}_L$ decreases with increasing Rm but still dominates when $Rm \simeq 400$, leading to Rm-dependent field strengths in simulations. The vertical line at $\chi = 0.1$ indicates the start of the LSD phase. (b) The fractional contribution from the dynamical term increases with increasing Rm with a power index 0.23. This implies T_D/\tilde{E}_L reaches 0.95 at $Rm = 3.5 \times 10^5$ if the relation can be extrapolated.

LSD phase, the LSD growth rate can become Rm independent at lower Rm than the value at which the mean-field strength becomes Rm independent. In the next subsection we explore the resistive effects on the LSD saturation.

B. Rm-dependent field strengths in simulations

The simulated values of \tilde{E}_L decrease with increasing Rm at fixed χ , as evident from Fig. 1. To quantify this, we define an exponent $p(\chi)$ by fitting the power-law $\tilde{E}_L(\chi, Rm) \propto Rm^{p(\chi)}$. We find that $p \simeq -0.5$ for all $\chi \in [0.01, 0.55]$, indicating that during the SSD phase and at all stages of the LSD, the mean-field energy decreases with increasing Rm. We now explain this dependence.

\tilde{E}_L can be inferred from the total magnetic helicity without integrating the growth equation. Consider the case where the volume-averaged magnetic helicity is zero initially, but later gains $\Delta H = H_1^M + H_2^M$ due to resistive diffusion, where $H_{1,2}^M$ are the average magnetic helicity of the large- and small-scale fields, respectively. Using Eq. (4) we have $H_1^M = s_1 k_1^{-1} \tilde{E}_L \rho u_{rms}^2$, and therefore

$$\tilde{E}_L(\chi, Rm) = -\frac{k_1}{s_1} \frac{H_2^M}{\rho u_{rms}^2} + \frac{k_1 \Delta H}{s_1 \rho u_{rms}^2}. \quad (20)$$

We denote the terms on the right of Eq. (20) by T_D and T_R , respectively, so that $\tilde{E}_L = T_D + T_R$. Note that T_R is from the resistive loss of magnetic helicity but T_D is purely dynamic. The resistive term does not amplify the large-scale field directly, but slows the growth of χ , thereby weakening the back reaction and allowing more large-scale growth. The ratio T_D/\tilde{E}_L determines whether resistive effects dominate and this is to be assessed below.

For all runs at all times, the magnetic fields at the resistive scale have positive magnetic helicity, whilst those at the lowest wave numbers have negative helicity. Hence $\Delta H < 0$ and $s_1 < 0$ always. As we discuss in detail in Appendix, $H_2^M < 0$ during the SSD phase, and hence $T_D/\tilde{E}_L < 0$ initially. In what follows we focus on the LSD phase when $H_2^M > 0$, the period during which T_D and T_R are both positive.

The evolution of T_D/\tilde{E}_L is shown in Fig. 3(a). The LSD starts to dominate the field growth at k_1 at $\chi \gtrsim 0.1$, and its back reaction on the small scales grows T_D . By the time $\chi =$

0.55 which is close to the end of the LSD regime, Eq. (20) determines how much the LSD has benefited from resistive contributions. That $T_D < T_R$ implies that the LSD quenching is still weakened substantially by the resistive dissipation of small-scale current helicity, and therefore the PQ regime depends strongly on Rm. This is why \tilde{E}_L decreases with increasing Rm at fixed χ .

IV. IMPLICATIONS FOR HIGHER Rm

In Fig. 3(b) we show the fractional contribution T_D/\tilde{E}_L at $\chi = 0.55$ versus Rm. A power-law relation $\propto Rm^{0.23}$ is found, but also notice that the trend flattens at large Rm. We now describe why this apparent saturation may not apply for much larger Rm, and why T_D might actually dominate at $\chi = 0.55$ as $Rm \rightarrow \infty$ and become Rm independent.

Since $T_R \propto \Delta H$ and is negligible during the LSD phase in the $Rm \rightarrow \infty$ limit, the necessary condition for an Rm-independent PQ regime is $dT_D/dRm \rightarrow 0$ as $Rm \rightarrow \infty$ (while its fractional contribution $T_D/\tilde{E}_L \rightarrow 1$ since $T_R \rightarrow 0$). In the LSD phase, the small-scale magnetic helicity spectrum \mathcal{H}_2^M is of one sign, so we write $T_D = -s_2 k_1 \chi^2 / s_1 k_2$. Since $|s_{1,2}| \simeq 1$ and k_1 is bounded from below, an Rm-independent PQ regime requires k_2 to depend at most weakly on Rm at fixed χ , which is determined by the magnetic helicity spectrum as explained below.

Consider a magnetic helicity spectrum $\mathcal{H}_2^M(k) \propto k^{-q}$ in the inertial range. This is appropriate for $Pm < 1$ flows. Using Eq. (9) for k_2 , we then have that $k_2/k_f = F(q-1)/F(q)$, where $F(x) = \int_1^r x^{-q} dx$, and r is the ratio between the dissipative scale of the helical fields and k_f . When $Rm \rightarrow \infty$, we have $r \gg 1$, so that $k_2/k_f = (q-1)/(q-2)$ when $q > 2$, but diverges for $q \leq 2$. Hence an Rm-independent PQ regime arises if $q > 2$.

For $Pm > 1$ flows whose magnetic energy and helicity spectra may have broken power laws at $k \geq k_f$, the conditions for an Rm-independent PQ regime become (i) a $q > 2$ range exists, and (ii) the wave number above which $q > 2$ does not increase with increasing Rm. Such evidence is indeed observed from our $Pm \geq 1$ simulations. For the two highest-Rm runs (at $Rm \simeq 250$ and 400), we find that the wave numbers at which $q - 2$ changes sign are both $\simeq 2k_f$ and do not scale with

Rm. This is consistent with previous indications that the peak wave number of the magnetic energy spectrum for large-Pm SSDs remains Rm independent for large Rm from both theory [42] and simulation [43]. Hence, our simulations imply an Rm-independent PQ regime for $\text{Pm} \geq 1$ flows.

We note that $\text{Re} = 5$ throughout our simulations, so the flow in the simulations is stochastic but not fully turbulent. At larger Re, the slope of the magnetic helicity spectrum will be affected by the more extended inertial range of the velocity field. The spectrum may also evolve from shallower than the aforementioned threshold at early times to steeper at later times. Then the influence of Rm on the saturated state could still be small, as is crudely suggested in a four-scale approach [39]. Future high-resolution simulations for both $\text{Pm} > 1$ and $\text{Pm} < 1$ are needed to concretely confirm the spectral slope of the magnetic helicity at large Re and Rm and its temporal evolution.

To summarize, for a magnetic helicity spectrum that satisfies the conditions mentioned three paragraphs above, the Rm-independent value that \tilde{E}_L can obtain at any χ is

$$\begin{aligned} \lim_{\text{Rm} \rightarrow \infty} \tilde{E}_L(\chi, \text{Rm}) &= \lim_{\text{Rm} \rightarrow \infty} T_D \\ &= -\frac{s_2}{s_1} \frac{k_1}{k_{\text{peak}}} \frac{q-2}{q-1} \chi^2, \end{aligned} \quad (21)$$

where k_{peak} is the Rm-independent peak of the magnetic helicity spectrum and $q > 2$ is the slope at $k \geq k_{\text{peak}}$.

Equation (21) is the lower bound for any case with finite Rm, to which the positive T_R term will additionally contribute. One caveat is that achieving this lower bound within a finite time is not guaranteed if the time to reach any given value of χ increases with Rm. In this case, T_D may not obtain any significant value as $\text{Rm} \rightarrow \infty$, even though $T_D/\tilde{E}_L \simeq 1$. This could happen if the SSD were to somehow suppress helicity generation at small scales, and in turn, slow large-scale dynamo growth through helicity conservation. However, at the Rm values explored in this work, we do not observe such evidence that SSD would suppress the growth of χ [see Fig. 1(b), which shows the opposite trend], but future higher-resolution simulations could help to further assess this.

For all of our simulation runs, we observe \tilde{E}_L is more than 12.5 times the lower bound Eq. (21) by taking $s_1/s_2 = -1$, $k_{\text{peak}} = 2k_f$, and $q = 8/3$, again highlighting the dominance of the resistive contribution. Furthermore, assuming $s_1/s_2 = -1$, $k_{\text{peak}} = 2k_f$, $q = 8/3$, $k_f/k_1 = 5$, and $\chi^2 = 1 - k_1/k_f$, we find this lower bound to be $\tilde{E}_L \simeq \langle B \rangle^2 / \langle b^2 \rangle = 0.032$, comparable to some observed galactic magnetic fields [44] which have benefited from the Rm-independent Ω effect and possible helicity fluxes. Hence, the DQ formalism predicts a substantial lower bound for the large-scale magnetic energy.

V. CONCLUSIONS

For astrophysical flows with $\text{Rm} \gg 1$, the saturation time of helical dynamos is resistively long, and fully saturated states are constrained by the resistive helicity loss [12,14] if there is no helicity flux. In this work, we use the normalized small-scale current helicity χ to track dynamo evolution in simulations and identify their LSD phases. We show that

(i) the onset of the LSD is marked by $\chi \geq 0.1$, independent of Rm; (ii) the LSD growth rate agrees well with the prediction of the DQ formalism in becoming Rm independent as $\text{Rm} \rightarrow \infty$; (iii) the LSD saturation at numerically accessible Rm values is still dominated by resistive contributions, but whether it becomes Rm independent as $\text{Rm} \rightarrow \infty$ depends on the slope of the magnetic current helicity spectrum.

Our results clarify that the decreasing saturation level of helical dynamos associated with increasing Rm in closed boxes is due to the decreasing resistive contribution, but this does not preclude convergence to a resistivity independent value for large Rm. For high-Rm α^2 or $\alpha^2\text{-}\Omega$ dynamos of stars and galaxies, our results imply that when the current helicity spectrum falls off with any positive power of k , efficient LSD growth is possible. This applies even without boundary helicity fluxes, including systems requiring Rm-independent cycle periods, although helicity fluxes may play a prominent role in the actual operation of dynamos in real systems. For shallower spectra, helicity fluxes or some non-helicity driven LSD, e.g., Ref. [45], would be needed to explain the observed field strengths, let alone fast-cycle periods. For planetary dynamos whose resistive time scales can be comparable to LSD dynamical times, α quenching is significantly weakened by resistive diffusion and so the LSD is much less constrained by the slope of the current helicity spectrum.

The results also highlight the broader importance of feedback between mean-field dynamo growth and MHD turbulent spectra as the latter itself may evolve due to the increasing large-scale magnetic field. The mutual evolution of turbulence, LSD, and outflows in spinning-down stars or accretion flows from LSD-mediated magnetic winds exemplifies that the implications of such feedback have direct observational consequences.

Data and post-processing programs for this article are available on Ref. [46].

ACKNOWLEDGMENTS

Nordita is sponsored by Nordforsk. We acknowledge allocation of computing resources from the Swedish National Allocations Committee at the Center for Parallel Computers at the Royal Institute of Technology in Stockholm and Linköping. Part of the numerical simulations in this work were carried out on the Astro cluster supported by Tsung-Dao Lee Institute at Shanghai Jiao Tong University. H.Z. acknowledges support from Grant No. 2023M732251 from the China Postdoctoral Science Foundation. E.B. acknowledges the Isaac Newton Institute for Mathematical Sciences, Cambridge, for support and hospitality during the program ‘‘Frontiers in dynamo theory: from the Earth to the stars.’’ This work was supported by EPSRC Grant No. EP/R014604/1. E.B. also acknowledges working in part at the Aspen Center for Physics, which is supported by National Science Foundation Grant No. PHY-2210452, and additional support from U.S. Department of Energy Grants No. DE-SC0001063, No. DE-SC0020432, No. DE-SC0020103, and U.S. NSF Grants No. AST-1813298 and No. PHY-2020249.

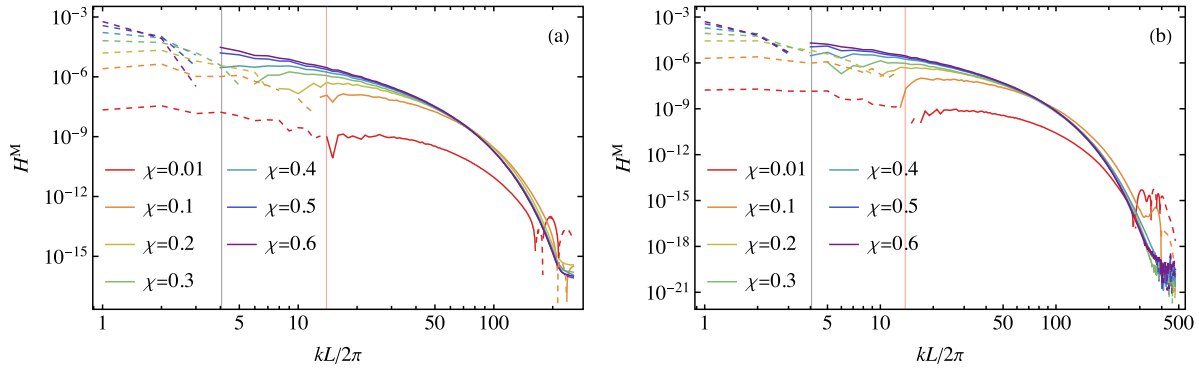


FIG. 4. Evolution of the magnetic helicity spectrum for runs (a) A5 at $\text{Rm} \simeq 250$ and (b) A6 at $\text{Rm} \simeq 400$, whose velocity fields are fully positively helical. Solid and dashed parts indicate positively and negatively helical modes, respectively. During the SSD phase ($\chi \leq 0.1$), the negatively helical magnetic field resides beyond the forcing wave number ($k_f = 4$ as indicated by the black vertical lines), in fact up to the viscous wave number ($k_v = \text{Re}^{3/4} k_f$ as indicated by the red vertical lines).

APPENDIX: HELICAL FIELDS DURING THE SSD PHASE

The evolution of T_D/\tilde{E}_L is shown in Fig. 3(a) in the main text. For the three runs with the highest Rm , we see $T_D/\tilde{E}_L < 0$ and therefore $T_R/\tilde{E}_L = 1 - T_D/\tilde{E}_L > 1$ during the SSD phase. Together with $s_1 < 0$, this implies a negative average handedness of the small-scale field $s_2 < 0$ [see Eqs. (8) and (20) in the main text]. This is because at that time, negative helicity resides on a wide range of k , particularly at both $k < k_f$ and a finite range at $k \geq k_f$; see Fig. 4. This implies that, since the field at k_1 is already fully helical, $k_1 \Delta H/s_1$ alone would overestimate the large-scale contribution, i.e., $T_R/\tilde{E}_L > 1$.

In fact, the initial dividing wave number k_{div} between the positively and negatively helical parts is not k_f , but roughly the viscous wave number k_v (Fig. 4). The SSD initially operates most efficiently on the viscous scale, and generates positively helical fields at $k > k_v$. Conservation of magnetic helicity requires that negatively signed magnetic helicity must compensate at $k < k_v$ at a generation rate comparable to that

of the efficient SSD at k_v . Thus, the net sign of helicity at $k < k_v$ is initially negative. As the SSD at k_v approaches saturation, its back reaction that produces negative helicity on larger scales eventually becomes slower than the SSD rate below k_v , and so positive helicity starts to build up there and we see k_{div} decreasing, until eventually it reaches $k_{\text{div}} = k_f$. Hence, $s_2 < 0$ during the kinematic SSD phase but becomes positive when the SSD saturates.

Although \tilde{E}_L decreases with increasing Rm at fixed χ in the simulation runs it is for different reasons in the SSD and LSD phases. In the SSD phase at $\chi \simeq 0.01$, the scaling $\tilde{E}_L \propto \text{Rm}^{-0.5}$ for our $\text{Pm} \geq 1$ cases is similar to the result of Refs. [47,48] that $\langle B \rangle/b_{\text{rms}} \propto \text{Rm}^{-3/4}$ for $\text{Pm} = 0.1$ cases. In fact, we find that the ratio $\langle B \rangle/b_{\text{rms}}$ is a constant at $\chi \leq 0.1$ for each run [see Fig. 1(c); roughly 300 eddy turnover times], but is $\propto \text{Rm}^{-1/2}$. That $\langle B \rangle$ and b_{rms} grow at the same rate is a signature of the SSD phase (or, in the language of Ref. [48], a feature of the kinematic dynamo phase), although the origin of $-1/2$ is not yet fully understood [47].

- [1] N. J. Wright, J. J. Drake, E. E. Mamajek, and G. W. Henry, The stellar-activity-rotation relationship and the evolution of stellar dynamos, *Astrophys. J.* **743**, 48 (2011).
- [2] R. Beck, Magnetic fields in spiral galaxies, *Astron. Astrophys. Rev.* **24**, 4 (2016).
- [3] A. Tchekhovskoy, R. Narayan, and J. C. McKinney, Efficient generation of jets from magnetically arrested accretion on a rapidly spinning black hole, *Mon. Not. R. Astron. Soc.* **418**, L79 (2011).
- [4] R. Fernández, A. Tchekhovskoy, E. Quataert, F. Foucart, and D. Kasen, Long-term GRMHD simulations of neutron star merger accretion discs: Implications for electromagnetic counterparts, *Mon. Not. R. Astron. Soc.* **482**, 3373 (2019).
- [5] E. N. Parker, Hydromagnetic dynamo models, *Astrophys. J.* **122**, 293 (1955).
- [6] M. Steenbeck, F. Krause, and K. H. Rädler, Berechnung der mittleren LORENTZ-Feldstärke für ein elektrisch leitendes Medium in turbulenter, durch CORIOLIS-Kräfte beeinflusster Bewegung, *Zeitschrift Naturforschung Teil A* **21**, 369 (1966).
- [7] H. K. Moffatt, *Magnetic Field Generation in Electrically Conducting Fluids* (Cambridge University Press, Cambridge, England, 1978).
- [8] K.-H. Rädler, N. Kleeorin, and I. Rogachevskii, The mean electromotive force for MHD turbulence: The case of a weak mean magnetic field and slow rotation, *Geophys. Astrophys. Fluid Dyn.* **97**, 249 (2003).
- [9] K.-H. Rädler and R. Stepanov, Mean electromotive force due to turbulence of a conducting fluid in the presence of mean flow, *Phys. Rev. E* **73**, 056311 (2006).
- [10] A. Brandenburg, The inverse cascade and nonlinear alpha-effect in simulations of isotropic helical hydromagnetic turbulence, *Astrophys. J.* **550**, 824 (2001).
- [11] E. G. Blackman and G. B. Field, New dynamical mean-field dynamo theory and closure approach, *Phys. Rev. Lett.* **89**, 265007 (2002).

- [12] A. Brandenburg and G. R. Sarson, Effect of hyperdiffusivity on turbulent dynamos with helicity, *Phys. Rev. Lett.* **88**, 055003 (2002).
- [13] S. Candelaesi and A. Brandenburg, Kinetic helicity needed to drive large-scale dynamos, *Phys. Rev. E* **87**, 043104 (2013).
- [14] G. Bermudez and A. Alexakis, Saturation of turbulent helical dynamos, *Phys. Rev. Lett.* **129**, 195101 (2022).
- [15] R. M. Kulsrud and S. W. Anderson, The spectrum of random magnetic fields in the mean field dynamo theory of the galactic magnetic field, *Astrophys. J.* **396**, 606 (1992).
- [16] F. Cattaneo and S. I. Vainshtein, Suppression of turbulent transport by a weak magnetic field, *Astrophys. J. Lett.* **376**, L21 (1991).
- [17] S. I. Vainshtein and F. Cattaneo, Nonlinear restrictions on dynamo action, *Astrophys. J.* **393**, 165 (1992).
- [18] A. V. Gruzinov and P. H. Diamond, Self-consistent theory of mean-field electrodynamics, *Phys. Rev. Lett.* **72**, 1651 (1994).
- [19] A. V. Gruzinov and P. H. Diamond, Self-consistent mean field electrodynamics of turbulent dynamos, *Phys. Plasmas* **2**, 1941 (1995).
- [20] A. V. Gruzinov and P. H. Diamond, Nonlinear mean field electrodynamics of turbulent dynamos, *Phys. Plasmas* **3**, 1853 (1996).
- [21] M. Ossendrijver, M. Stix, and A. Brandenburg, Magnetoconvection and dynamo coefficients: Dependence of the alpha effect on rotation and magnetic field, *Astron. Astrophys.* **376**, 713 (2001).
- [22] S. M. Tobias and F. Cattaneo, Shear-driven dynamo waves at high magnetic Reynolds number, *Nature (London)* **497**, 463 (2013).
- [23] E. G. Blackman and G. B. Field, Constraints on the magnitude of α in dynamo theory, *Astrophys. J.* **534**, 984 (2000).
- [24] E. T. Vishniac and J. Cho, Magnetic helicity conservation and astrophysical dynamos, *Astrophys. J.* **550**, 752 (2001).
- [25] K. Subramanian and A. Brandenburg, Nonlinear current helicity fluxes in turbulent dynamos and alpha quenching, *Phys. Rev. Lett.* **93**, 205001 (2004).
- [26] A. Hubbard and A. Brandenburg, Catastrophic quenching in $\alpha\Omega$ dynamos revisited, *Astrophys. J.* **748**, 51 (2012).
- [27] F. Rincon, Helical turbulent nonlinear dynamo at large magnetic Reynolds numbers, *Phys. Rev. Fluids* **6**, L121701 (2021).
- [28] K. Gopalakrishnan and K. Subramanian, Magnetic helicity fluxes from triple correlators, *Astrophys. J.* **943**, 66 (2023).
- [29] P. Bhat, Saturation of large-scale dynamo in anisotropically forced turbulence, *Mon. Not. R. Astron. Soc.* **509**, 2249 (2022).
- [30] A. Brandenburg and K. Subramanian, Astrophysical magnetic fields and nonlinear dynamo theory, *Phys. Rep.* **417**, 1 (2005).
- [31] A. Brandenburg, Advances in mean-field dynamo theory and applications to astrophysical turbulence, *J. Plasma Phys.* **84**, 735840404 (2018).
- [32] D. W. Hughes, Mean field electrodynamics: Triumphs and tribulations, *J. Plasma Phys.* **84**, 735840407 (2018).
- [33] F. Rincon, Dynamo theories, *J. Plasma Phys.* **85**, 205850401 (2019).
- [34] A. Brandenburg and E. Ntormousi, Galactic dynamos, *Annu. Rev. Astron. Astrophys.* **61**, 561 (2023).
- [35] J. Pietarila Graham, E. G. Blackman, P. D. Mininni, and A. Pouquet, Not much helicity is needed to drive large-scale dynamos, *Phys. Rev. E* **85**, 066406 (2012).
- [36] P. Bhat, K. Subramanian, and A. Brandenburg, Efficient quasi-kinematic large-scale dynamo as the small-scale dynamo saturates, [arXiv:1905.08278](https://arxiv.org/abs/1905.08278) [astro-ph.GA].
- [37] A. Pouquet, U. Frisch, and J. Leorat, Strong MHD helical turbulence and the nonlinear dynamo effect, *J. Fluid Mech.* **77**, 321 (1976).
- [38] N. I. Kleeorin and A. A. Ruzmaikin, Dynamics of the average turbulent helicity in a magnetic field, *Magnetohydrodynamics* **18**, 116 (1982) [Translation from *Magnitnaya Gidrodinamika* **2**, 17 (1982)].
- [39] E. G. Blackman, Understanding helical magnetic dynamo spectra with a non-linear four-scale theory, *Mon. Not. R. Astron. Soc.* **344**, 707 (2003).
- [40] A. Brandenburg, K.-H. Rädler, M. Rheinhardt, and K. Subramanian, Magnetic quenching of α and diffusivity tensors in Helical turbulence, *ApJL* **687**, L49 (2008).
- [41] Pencil Code Collaboration, A. Brandenburg, A. Johansen, P. Bourdin, W. Dobler, W. Lyra, M. Rheinhardt, S. Bingert, N. Haugen, A. Mee, F. Gent, N. Babkovskaia, C.-C. Yang, T. Heinemann, B. Dintrans, D. Mitra, S. Candelaesi, J. Warnecke, P. Käpylä, A. Schreiber *et al.*, The Pencil Code, a modular MPI code for partial differential equations and particles: Multipurpose and multiuser-maintained, *J. Open Source Softw.* **6**, 2807 (2021).
- [42] K. Subramanian, Unified treatment of small- and large-scale dynamos in helical turbulence, *Phys. Rev. Lett.* **83**, 2957 (1999).
- [43] A. K. Galishnikova, M. W. Kunz, and A. A. Schekochihin, Tearing instability and current-sheet disruption in the turbulent dynamo, *Phys. Rev. X* **12**, 041027 (2022).
- [44] R. Beck, L. Chamandy, E. Elson, and E. G. Blackman, Synthesizing observations and theory to understand galactic magnetic fields: Progress and challenges, *Galaxies* **8**, 4 (2019).
- [45] V. Skoutnev, J. Squire, and A. Bhattacharjee, On large-scale dynamos with stable stratification and the application to stellar radiative zones, *Mon. Not. R. Astron. Soc.* **517**, 526 (2022).
- [46] H. Zhou and E. Blackman, Dataset for “Helical dynamo growth at modest versus extreme magnetic Reynolds numbers” (v2023.02.12) [Data set], [Zenodo](https://zenodo.org/doi/10.5281/zenodo.7632994), doi:10.5281/zenodo.7632994.
- [47] K. Subramanian and A. Brandenburg, Traces of large-scale dynamo action in the kinematic stage, *Mon. Not. R. Astron. Soc.* **445**, 2930 (2014).
- [48] P. Bhat, K. Subramanian, and A. Brandenburg, A unified large/small-scale dynamo in helical turbulence, *Mon. Not. R. Astron. Soc.* **461**, 240 (2016).